

A fast direct solver for two dimensional quasi-periodic multilayered medium scattering problems

Y. Zhang, and A. Gillman

Abstract: This manuscript presents a fast direct solution technique for solving two dimensional wave scattering problems from quasi-periodic multilayered structures. A boundary integral formulation that is robust at Wood's anomalies is used to represent the solution within a infinite strip in the direction of the periodicity. Rayleigh-Bloch expansions are used to represent the solution outside the strip and satisfy the radiation condition. A block sparse linear system results from enforcing continuity of the solution through the interfaces, the quasi-periodicity of the solution and its flux as well as continuity of the solution inside an outside the infinite strip. When the interface geometries are complex, the linear system is too large to be handled via dense linear algebra. The key building block of the proposed solver is a fast direct direct solver for the large sparse block system that corresponds to the discretization of boundary integral equations. The solver makes use of hierarchical matrix inversion techniques, has a cost that scales linearly with respect to the number of unknowns on the interfaces and the precomputation can be used for all choices of boundary data. By partitioning the remainder of the precomputation into parts based on their dependence on incident angle, the proposed direct solver is efficient for problems involving many incident angles like those that arise in applications. For example for a problem on an eleven layer geometry where the solution is desired for 287 incident angles, the proposed solution technique is 87 times faster than building a new fast direct solver for each new incident angle. An additional feature of the proposed solution technique is that solving a problem where an interface or layer property is changed require an update in the precomputation that cost linearly with respect to the number points on the affected interfaces with a small constant prefactor. The efficiency for modified geometries and multiple solves make the solution technique well suited for optimal design and inverse scattering applications.

1. INTRODUCTION

This manuscript considers the $I + 1$ layered scattering problem defined by

$$\begin{aligned}
 (\Delta + \omega_i^2)u_i(\mathbf{x}) &= 0 & \mathbf{x} \in \Omega_i \\
 u_1 - u_2 &= -u^{\text{inc}}(\mathbf{x}) & \mathbf{x} \in \Gamma_1 \\
 \frac{\partial u_1}{\partial \nu} - \frac{\partial u_2}{\partial \nu} &= -\frac{\partial u^{\text{inc}}}{\partial \nu} & \mathbf{x} \in \Gamma_1 \\
 u_i - u_{i+1} &= 0 & \mathbf{x} \in \Gamma_i, 1 < i < I + 1 \\
 \frac{\partial u_i}{\partial \nu} - \frac{\partial u_{i+1}}{\partial \nu} &= 0 & \mathbf{x} \in \Gamma_i, 1 < i < I + 1
 \end{aligned}
 \tag{1.1}$$

where u_i is the unknown solution in the region $\Omega_i \in \mathbb{R}^2$ where the wave number is given by ω_i for $i = 1, \dots, I+1$. The interface Γ_i for $i = 1, \dots, I$ between each layer is periodic with period d . The boundary conditions enforce continuity of the solution and its flux through the interfaces Γ_i . The incident wave u^{inc} is defined by $u^{\text{inc}}(\mathbf{x}) = e^{i\mathbf{k} \cdot \mathbf{x}}$ where the incident vector is $\mathbf{k} = (\omega_1 \cos \theta^{\text{inc}}, \omega_1 \sin \theta^{\text{inc}})$ and the incident angle is $-\pi < \theta^{\text{inc}} < 0$. Figure 1.1 illustrates a five layered periodic geometry. The incident wave u^{inc} is *quasi-periodic* up to a phase, i.e. $u^{\text{inc}}(x + d, y) = \alpha u^{\text{inc}}(x, y)$ for $(x, y) \in \mathbb{R}^2$, where α is the Bloch phase defined by

$$\alpha := e^{i\omega_1 d \cos \theta^{\text{inc}}}.$$

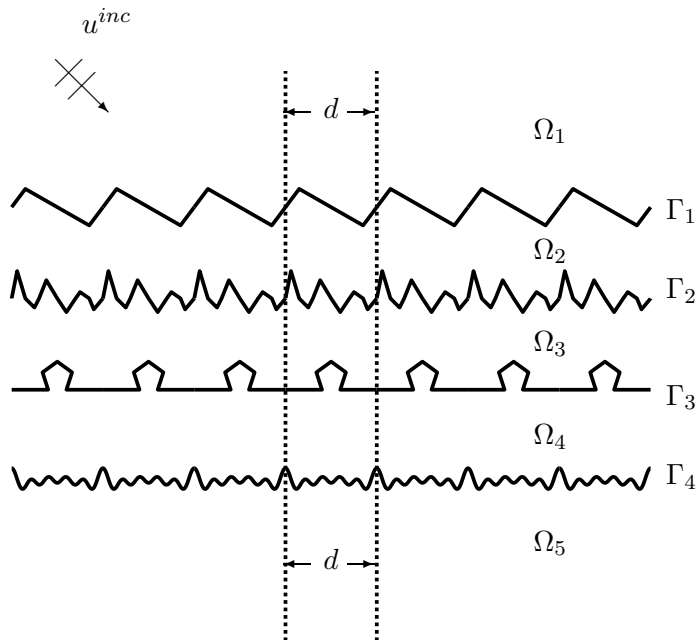


FIGURE 1.1. A five layered periodic geometry. 7 periods are shown.

Multilayered periodic geometries are important in the design of optical and electromagnetic devices as well as select inverse scattering applications. Some specific devices that involve scattering from multi-layered medium are solar cells (thin-film photovoltaic cells [3, 28] and solar thermal power [38]), dielectric gratings for high-powered laser [36, 6] and wideband [26] applications. Most of these applications require solving a scattering problem for a large number of incident angles θ^{inc} . For example, in many engineering applications, a Bragg diagram created from the solution of 200 boundary value problems is desirable. In optimal design applications and inverse scattering, solving a scattering problem is nested inside of an optimization loop. At each step in the loop, a new scattering problem needs to be solved for many incident angles. When the geometry and material properties are close to the optimal choice or there are sufficient constraints on the material and/or interface properties the changes in the scattering problem are localized to a few layer.

This paper presents a fast direct solver for the multilayered medium integral equation formulation presented in [14]. This integral formulation is robust even at so-called Wood's anomalies. The computational cost of the proposed fast direct solver scales linearly with respect to the number of discretization points on the interfaces. When a layer is changed with new material properties and/or a new interface, the cost of updating the direct solver scales linearly with respect to the number of discretization points affected by the modification. For changing an interface, updating the direct solver has a cost that scales linearly with respect to the number of discretization points on the new interface. For updating a wave speed in Ω_i , the cost scales linearly with respect to the number of discretization points on the interfaces bounding Ω_i . This makes the solution technique a good option for design and inverse scattering applications.

1.1. Related work. Direct discretization of (1.1) is possible via finite difference or finite element methods [25] but it faces two challenges, (i) meshing to the interfaces to maintain

accuracy and (ii) enforcing the radiation condition. Meshing can be effectively be handled using mesh generation software such as GMESH [16]. Techniques such as perfectly matched layers [30] can artificially enforce radiation conditions but lose accuracy if the points per wavelength remains fixed (the so-called *pollution* effect) [4]. Another alternative method for directly discretizing (1.1) is the rigorous-coupled wave analysis (RCWA) or Fourier Modal Method. It is designed for multilayer gratings [34] which is dependent on an iterative solve. While a Fourier factorization method [32, 31] can be used to accelerate convergence of an iterative solver, this solution approach is not ideal for problems with many right hand sides that arise in applications. An additional challenge of RCWA is that it is difficult to apply to arbitrary shaped interfaces.

When each layer is comprised of constant coefficient (i.e. not heterogeneous) medium, it is possible to recast (1.1) as a collection of boundary integral equations where the unknowns lie on the interfaces between layers. A boundary integral technique utilizing a fast direct solver for two layered medium where one of the layers has inclusions was presented in [19]. The integral formulation utilized the quasi-periodic Green’s function which is defined as an infinite series. For some choices of boundary data, this series does not converge even though the problem is well posed. An incident angle θ^{inc} that causes the quasi-periodic Green’s function not to converge is called a *Wood’s anomaly*. There have been many techniques suggested to avoid these anomalies (such as [5, 11]). This paper will build on the robust integral formulation in [14] though it is likely possible to build similar direct solvers for other formulations that are robust at Wood’s anomalies. The integral formulation in [14] makes use of the free space Helmholtz Green’s function, avoids the infinite sum and uses auxiliary unknowns to enforce periodicity. By coupling the integral formulation to Rayleigh-Bloch expansions, the solution technique automatically satisfies the radiation condition. Recently, [13] replaced the boundary integral formulation in this approach to a techniques based on the method of fundamental solutions. This exchanges a second kind integral equation for a formulation that results in a system that is exponentially ill-conditioned.

1.2. High level view of solution technique. Due to the problems associated with the quasi-periodic Green’s function and our desire to exploit the constant coefficient medium, the fast direct solver is built for the robust boundary integral formulation proposed in [14]. Each interface has a boundary integral equation that has “structural” similarities to a boundary integral equation for scattering off a single geometry. The structural similarity is the fact that a block matrix in the discretized boundary integral equation is amenable to fast direct inversion techniques such as *Hierarchically Block Separable (HBS)* methods [17, 23, 10] which are closely related to the *Hierarchically Semi-Separable (HSS)* [41, 39, 40], the Hierarchical interpolative factorization [24], the \mathcal{H} and \mathcal{H}^2 -matrix methods [7, 8]. Roughly speaking these fast direct solvers utilize the fact that the off-diagonal blocks of the discretized integral equation are low rank to create compressed representations of the matrix and its inverse.

The linear system resulting from the discretization of the integral formulation in [14] is rectangular where the principle subblock is a block tridiagonal matrix. Each block in this tridiagonal matrix corresponds to a discretized boundary integral operator and (in the low frequency regime) is amenable to compression techniques such as those in fast direct solvers. Utilizing this and separating the matrices that depend on Bloch phase allows for the precomputation of the direct solver to be utilized for all choices of incident angle. The Bloch phase dependence of many of the other block matrices in the rectangular system can be separated out in a similar manner allowing them to be reused for multiple solves. Further acceleration is gained by exploiting the block diagonal or nearly block diagonal sparsity

pattern of all the matrices. The combination of all these efforts dramatically reduces the cost of processing the many solves needed in applications.

1.3. Outline. The paper begins by reviewing the integral formulation from [14] in section 2. Next, section 3 presents the proposed fast direct solver. Numerical results in section 4 illustrate the performance of the direct solver. Section 5 summarizes manuscript and reviews the key features of the presented work.

2. PERIODIZING SCHEME

This section provides a review of the boundary integral formulation presented in [14]. The necessary integral operators are presented in 2.1. Then the full representation is presented in 2.2. Finally, the linear system resulting from enforcing continuity and quasi-periodicity of the solution is presented in section 2.3.

The integral formulation proposed in [14] solves (1.1) in an infinite vertical unit strip of width d . Because the solution is known to be quasi-periodic, the solution outside of the unit strip can be found by scaling the solution by the appropriate Bloch phase factor. Let $x = L$ and $x = R$ denote the left and right bounds for the unit strip. The solution technique further partitions space by introducing artificial top and bottom partitions to the unit strip at $y = y_U$ and $y = y_D$ respectively. Figure 2.1(a) illustrates this partitioning. The box bounded by these artificial boundaries is called the *unit cell*. Inside the unit cell the solution is represented via an integral formulation. Above and below the unit cell, (i.e. for points in the unit strip where $y > y_U$ and $y < y_D$), the solution is given by Raleigh-Bloch expansions. Specifically, for $\mathbf{x} = (x, y)$ in the unit strip where $y > y_U$, the solution is given by

$$(2.1) \quad u(x, y) = \sum_{n \in \mathbb{Z}} a_n^U e^{i\kappa_n x} e^{ik_n^U (y - y_U)}$$

and, for $\mathbf{x} = (x, y)$ in the unit strip where $y < y_D$, the solution is given by

$$(2.2) \quad u(x, y) = \sum_{n \in \mathbb{Z}} a_n^D e^{i\kappa_n x} e^{ik_n^D (-y + y_D)}$$

where $\kappa_n := \omega_1 \cos \theta^{\text{inc}} + \frac{2\pi n}{d}$, $k_n^U = \sqrt{\omega_1^2 - \kappa_n^2}$, $k_n^D = \sqrt{\omega_{I+1}^2 - \kappa_n^2}$ and the sets $\{a_n^U\}$ and $\{a_n^D\}$ are coefficients to be determined.

2.1. Integral operators. This section presents the integral operators needed to represent the solution inside the unit cell.

Let Γ_i for $i = 1, \dots, I$ denote the interfaces inside the unit cell and Ω_i denote the regions in between each layer in the unit cell. Both are numbered from the top down. Figure 2.1(a) illustrates the numbering of the five layered geometry within the unit cell.

Let $G_\omega(\mathbf{x}, \mathbf{y}) = \frac{i}{4} H_0^{(1)}(\omega \|\mathbf{x} - \mathbf{y}\|)$ denote the two dimensional free space Green's function for the Helmholtz equation with wave number ω where H_0^1 is the Hankel function of zeroth order [1].

The standard Helmholtz single and double layer integral operators defined on a curve W [15] are

$$(\mathcal{S}_W^\omega \rho)(\mathbf{x}) = \int_W G_\omega(\mathbf{x}, \mathbf{y}) \rho(\mathbf{y}) dl(\mathbf{y}) \quad (\mathcal{D}_W^\omega \rho)(\mathbf{x}) = \int_W \partial_{\nu_{\mathbf{y}}} G_\omega(\mathbf{x}, \mathbf{y}) \rho(\mathbf{y}) dl(\mathbf{y}),$$

respectively, where $\nu_{\mathbf{y}}$ denotes the normal vector at the point $\mathbf{y} \in W$.

For the periodizing scheme, integral operators involving the unit cell and its neighbors (left and right) are needed.

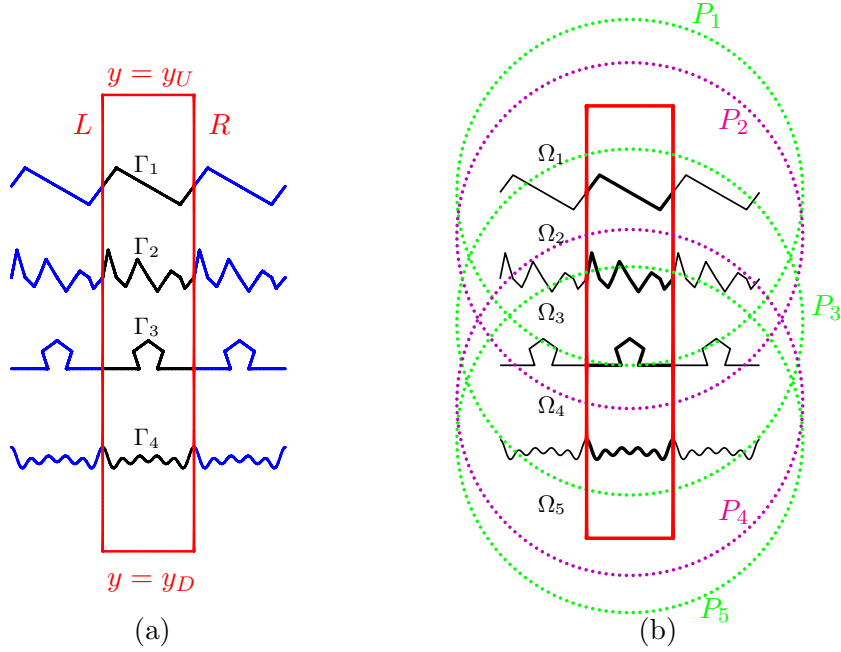


FIGURE 2.1. This figure is an illustration of a five layered periodic geometry with artificial walls and proxy circles. Only three periods of the infinite periodic geometry are shown. The period contained within the unit cell is in black while the other two periods are in blue. Figure (a) illustrates the notation for the unit cell with left, right, upper, and lower boundary L , R , U , and D shown in red lines. Figure (b) illustrates the proxy circles P_i for each layer. The color of the proxy circles alternates between green and magenta.

These operators, denoted with tilde, are defined as follows

$$(2.3) \quad \begin{aligned} (\tilde{\mathcal{S}}_W^\omega \rho)(\mathbf{x}) &= \sum_{l=-1}^1 \alpha^l \int_W G_\omega(\mathbf{x}, \mathbf{y} + l\mathbf{d}) \rho(\mathbf{y}) dl(\mathbf{y}) \\ &= (\mathcal{S}_W^\omega \rho)(\mathbf{x}) + (\mathcal{S}_{pm,W}^\omega \rho)(\mathbf{x}) \end{aligned}$$

and

$$(2.4) \quad \begin{aligned} (\tilde{\mathcal{D}}_W^\omega \rho)(\mathbf{x}) &= \sum_{l=-1}^1 \alpha^l \int_W \partial_{\nu_y} G_\omega(\mathbf{x}, \mathbf{y} + l\mathbf{d}) \rho(\mathbf{y}) dl(\mathbf{y}) \\ &= (\mathcal{D}_W^\omega \rho)(\mathbf{x}) + (\mathcal{D}_{pm,W}^\omega \rho)(\mathbf{x}) \end{aligned}$$

where

$$(2.5) \quad (\mathcal{S}_{pm,W}^\omega \rho)(\mathbf{x}) = \sum_{l=-1, l \neq 0}^1 \alpha^l \int_W G_\omega(\mathbf{x}, \mathbf{y} + l\mathbf{d}) \rho(\mathbf{y}) dl(\mathbf{y})$$

and

$$(2.6) \quad (\mathcal{D}_{pm,W}^\omega \rho)(\mathbf{x}) = \sum_{l=-1, l \neq 0}^1 \alpha^l \int_W \partial_{\nu_y} G_\omega(\mathbf{x}, \mathbf{y} + l\mathbf{d}) \rho(\mathbf{y}) dl(\mathbf{y}).$$

These integral operators are not sufficient to enforce quasi-periodicity. They are missing information from the infinite copies that are “far” from the unit cell. A proxy basis is used to capture the missing information. For simplicity, consider a layer Ω_l . Let $\{\mathbf{y}_j\}_{j=1}^P$ denote a collection of uniformly distributed points on a circle P_l of radius $2d$ that is centered in Ω_l . The elements of the *proxy basis* used to capture far field information are defined by

$$(2.7) \quad \phi_j^{\omega_l} = \frac{\partial G_{\omega_l}}{\partial \mathbf{n}_j}(\mathbf{x}, \mathbf{y}_j) + i\omega_l G_{\omega_l}(\mathbf{x}, \mathbf{y}_j)$$

where \mathbf{n}_j is the normal vector at \mathbf{y}_j on P_l . If the layer has a high aspect ratio (i.e. taller than d), the proxy surface should be taken to be an ellipse; see page 8 of [14]. Figure 2.1(b) illustrates the proxy circles for a five layered geometry.

The boundary integral equations involve additional integral operators which we define in this section for simplicity of presentation. Specifically, an integral operator defined on an interface W will need to be evaluated at $\mathbf{x} \in V$ where V is an interface (the same or a vertical neighbor).

For $\mathbf{x} \in V$ where V is an interface, let $(\tilde{S}_{V,W}^\omega \rho)$ denote the evaluation of (2.3) at \mathbf{x} , i.e.

$$(\tilde{S}_{V,W}^\omega \rho)(\mathbf{x}) = \sum_{l=-1}^1 \alpha^l \int_W G_\omega(\mathbf{x}, \mathbf{y} + l\mathbf{d}) \rho(\mathbf{y}) dl(\mathbf{y}).$$

Likewise, let $(\tilde{D}_{V,W}^\omega \rho)$ denote the evaluation of (2.3) at $\mathbf{x} \in V$, i.e.

$$(\tilde{D}_{V,W}^\omega \rho)(\mathbf{x}) = \sum_{l=-1}^1 \alpha^l \int_W \partial_{\nu_{\mathbf{y}}} G_\omega(\mathbf{x}, \mathbf{y} + l\mathbf{d}) \rho(\mathbf{y}) dl(\mathbf{y}).$$

The *pm* notation for the neighbor interactions follows in a similar fashion, for example the $(\tilde{S}_{V,W}^\omega \rho)(\mathbf{x})$ can be written as the following sum

$$(\tilde{S}_{V,W}^\omega \rho)(\mathbf{x}) = (S_{V,W}^\omega \rho)(\mathbf{x}) + (S_{V,\{pm,W\}}^\omega \rho)(\mathbf{x}),$$

where

$$(S_{V,\{pm,W\}}^\omega \rho)(\mathbf{x}) = \sum_{l=-1, l \neq 0}^1 \alpha^l \int_W G_\omega(\mathbf{x}, \mathbf{y} + l\mathbf{d}) \rho(\mathbf{y}) dl(\mathbf{y}).$$

In order to enforce continuity of the fluxes, the normal derivatives of these integral operators are required. For $\mathbf{x} \in V$ where V is an interface, let $(\tilde{D}_{W,V}^{*,\omega} \rho)$ denote the evaluation of the normal derivative of the single layer operator (2.3) at \mathbf{x} , i.e.

$$(\tilde{D}_{W,V}^{*,\omega} \rho)(\mathbf{x}) = \sum_{l=-1}^1 \alpha^l \int_W \partial_{\nu_{\mathbf{x}}} \partial_{\nu_{\mathbf{y}}} G_\omega(\mathbf{x}, \mathbf{y} + l\mathbf{d}) \rho(\mathbf{y}) dl(\mathbf{y})$$

where $\nu_{\mathbf{x}}$ is the normal vector at $\mathbf{x} \in V$. Similarly, let $(\tilde{T}_{W,V}^\omega \rho)$ denote the evaluation of the normal derivative of the double layer operator (2.4) at \mathbf{x} , i.e.

$$(\tilde{T}_{W,V}^\omega \rho)(\mathbf{x}) = \sum_{l=-1}^1 \alpha^l \int_W \partial_{\nu_{\mathbf{x}}} \partial_{\nu_{\mathbf{y}}} G_\omega(\mathbf{x}, \mathbf{y} + l\mathbf{d}) \rho(\mathbf{y}) dl(\mathbf{y}).$$

2.2. Integral formulation. The periodizing scheme within the unit cell is based on a modified Müller-Rokhlin boundary integral formulation [35, 37]. Specifically, the solution in the unit cell is expressed as

$$(2.8) \quad u_1(\mathbf{x}) = (\tilde{S}_{\Gamma_1}^{\omega_1} \sigma_1)(\mathbf{x}) + (\tilde{D}_{\Gamma_1}^{\omega_1} \tau_1)(\mathbf{x}) + \sum_{j=1}^P c_j^1 \phi_j^{\omega_1}(\mathbf{x}) \quad \text{for } \mathbf{x} \in \Omega_1,$$

(2.9)

$$u_{I+1}(\mathbf{x}) = (\tilde{S}_{\Gamma_I}^{\omega_{I+1}} \sigma_I)(\mathbf{x}) + (\tilde{D}_{\Gamma_I}^{\omega_{I+1}} \tau_I)(\mathbf{x}) + \sum_{j=1}^P c_j^{I+1} \phi_j^{\omega_{I+1}}(\mathbf{x}) \quad \text{for } \mathbf{x} \in \Omega_{I+1},$$

$$(2.10) \quad u_i(\mathbf{x}) = (\tilde{S}_{\Gamma_{i-1}}^{\omega_i} \sigma_{i-1})(\mathbf{x}) + (\tilde{D}_{\Gamma_{i-1}}^{\omega_i} \tau_{i-1})(\mathbf{x}) + (\tilde{S}_{\Gamma_i}^{\omega_i} \sigma_i)(\mathbf{x}) + (\tilde{D}_{\Gamma_i}^{\omega_i} \tau_i)(\mathbf{x}) + \sum_{j=1}^P c_j^i \phi_j^{\omega_i}(\mathbf{x})$$

for $\mathbf{x} \in \Omega_i$, $2 \leq i \leq I$ where σ_i and τ_i are unknown boundary charge distributions and $\{c_j^i\}_{j=1}^P$ are unknown constants, for $i = 1, \dots, I$.

The three following boundary integral equations result from enforcing the Dirichlet boundary conditions in equation (1.1):

$$(2.11) \quad \begin{aligned} & -\tau_1 + (\tilde{D}_{\Gamma_1, \Gamma_1}^{\omega_1} - \tilde{D}_{\Gamma_1, \Gamma_1}^{\omega_2})\tau_1 + (\tilde{S}_{\Gamma_1, \Gamma_1}^{\omega_1} - \tilde{S}_{\Gamma_1, \Gamma_1}^{\omega_2})\sigma_1 - \tilde{D}_{\Gamma_1, \Gamma_2}^{\omega_2}\tau_2 - \tilde{S}_{\Gamma_1, \Gamma_2}^{\omega_2}\sigma_2 \\ & + \sum_{p=1}^P (c_p^1 \phi_p^{\omega_1} - c_p^2 \phi_p^{\omega_2})|_{\Gamma_1} = -u^{\text{inc}} \quad \text{on } \Gamma_1, \end{aligned}$$

$$(2.12) \quad \begin{aligned} & -\tau_I + (\tilde{D}_{\Gamma_I, \Gamma_I}^{\omega_I} - \tilde{D}_{\Gamma_I, \Gamma_I}^{\omega_{I+1}})\tau_I + (\tilde{S}_{\Gamma_I, \Gamma_I}^{\omega_I} - \tilde{S}_{\Gamma_I, \Gamma_I}^{\omega_{I+1}})\sigma_I - \tilde{D}_{\Gamma_I, \Gamma_{I-1}}^{\omega_{I+1}}\tau_{I-1} - \tilde{S}_{\Gamma_I, \Gamma_{I-1}}^{\omega_{I-1}}\sigma_{I-1} \\ & + \sum_{p=1}^P (c_p^I \phi_p^{\omega_I} - c_p^{I+1} \phi_p^{\omega_{I+1}})|_{\Gamma_I} = 0 \quad \text{on } \Gamma_I, \end{aligned}$$

and

$$(2.13) \quad \begin{aligned} & -\tau_i + (\tilde{D}_{\Gamma_i, \Gamma_i}^{\omega_i} - \tilde{D}_{\Gamma_i, \Gamma_i}^{\omega_{i+1}})\tau_i + (\tilde{S}_{\Gamma_i, \Gamma_i}^{\omega_i} - \tilde{S}_{\Gamma_i, \Gamma_i}^{\omega_{i+1}})\sigma_i + \tilde{D}_{\Gamma_i, \Gamma_{i-1}}^{\omega_i}\tau_{i-1} + \tilde{D}_{\Gamma_i, \Gamma_{i+1}}^{\omega_{i+1}}\tau_{i+1} + \\ & \tilde{S}_{\Gamma_i, \Gamma_{i-1}}^{\omega_i}\sigma_{i-1} + \tilde{S}_{\Gamma_i, \Gamma_{i+1}}^{\omega_{i+1}}\sigma_{i+1} + \sum_{p=1}^P (c_p^i \phi_p^{\omega_i} - c_p^{i+1} \phi_p^{\omega_{i+1}})|_{\Gamma_i} = 0 \quad \text{on } \Gamma_i \quad \text{for } 1 < i < I \end{aligned}$$

where $\tilde{S}_{\Gamma_{i+1}, \Gamma_i}^{\omega_i}$ denotes the periodize single layer integral operator (2.3) defined on Γ_i evaluated on Γ_{i+1} , etc.

Likewise, enforcing the Neumann boundary conditions in equation (1.1) on the interfaces results in the following boundary integral equations:

$$(2.14) \quad \begin{aligned} & -\sigma_1 + (\tilde{T}_{\Gamma_1, \Gamma_1}^{\omega_1} - \tilde{T}_{\Gamma_1, \Gamma_1}^{\omega_2})\tau_1 + (\tilde{D}_{\Gamma_1, \Gamma_1}^{*, \omega_1} - \tilde{D}_{\Gamma_1, \Gamma_1}^{*, \omega_2})\sigma_1 - \tilde{T}_{\Gamma_1, \Gamma_2}^{\omega_2}\tau_2 - \tilde{D}_{\Gamma_1, \Gamma_2}^{*, \omega_2}\sigma_2 \\ & + \sum_{p=1}^P \left(c_p^1 \frac{\partial \phi_p^{\omega_1}}{\partial \nu} - c_p^2 \frac{\partial \phi_p^{\omega_2}}{\partial \nu} \right) |_{\Gamma_1} = -u^{\text{inc}} \quad \text{on } \Gamma_1, \end{aligned}$$

$$\begin{aligned}
(2.15) \quad & -\sigma_I + (\tilde{T}_{\Gamma_I, \Gamma_I}^{\omega_I} - \tilde{T}_{\Gamma_I, \Gamma_I}^{\omega_{I+1}})\tau_I + (\tilde{D}_{\Gamma_I, \Gamma_I}^{*, \omega_I} - \tilde{D}_{\Gamma_I, \Gamma_I}^{*, \omega_{I+1}})\sigma_I - \tilde{T}_{\Gamma_I, \Gamma_{I-1}}^{\omega_{I+1}}\tau_{I-1} - \tilde{D}_{\Gamma_I, \Gamma_{I-1}}^{*, \omega_{I-1}}\sigma_{I-1} \\
& + \sum_{p=1}^P \left(c_p^I \frac{\partial \phi_p^{\omega_I}}{\partial \nu} - c_p^{I+1} \frac{\partial \phi_p^{\omega_{I+1}}}{\partial \nu} \right) |_{\Gamma_I} = 0 \text{ on } \Gamma_I,
\end{aligned}$$

and

$$\begin{aligned}
(2.16) \quad & -\sigma_i + (\tilde{T}_{\Gamma_i, \Gamma_i}^{\omega_i} - \tilde{T}_{\Gamma_i, \Gamma_i}^{\omega_{i+1}})\tau_i + (\tilde{D}_{\Gamma_i, \Gamma_i}^{*, \omega_i} - \tilde{D}_{\Gamma_i, \Gamma_i}^{*, \omega_{i+1}})\sigma_i + \tilde{T}_{\Gamma_i, \Gamma_{i-1}}^{\omega_i}\tau_{i-1} + \tilde{T}_{\Gamma_i, \Gamma_{i+1}}^{\omega_{i+1}}\tau_{i+1} \\
& + \tilde{D}_{\Gamma_i, \Gamma_{i-1}}^{*, \omega_i}\sigma_{i-1} + \tilde{D}_{\Gamma_i, \Gamma_{i+1}}^{*, \omega_{i+1}}\sigma_{i+1} + \sum_{p=1}^P \left(c_p^i \frac{\partial \phi_p^{\omega_i}}{\partial \nu} - c_p^{i+1} \frac{\partial \phi_p^{\omega_{i+1}}}{\partial \nu} \right) |_{\Gamma_i} = 0 \text{ on } \Gamma_i \text{ for } 1 < i < I.
\end{aligned}$$

2.3. Linear system. Once the representation of the solution has been determined and the boundary integral equations derived, the unknown densities, periodicity constants c_j^i for the proxy surfaces and the coefficients of the Rayleigh-Bloch expansion need to be approximated. This is done by approximating the boundary integral equations, the quasi-periodicity of the solution and its flux on the left and right walls, and the continuity of the solution through the top and bottom of the unit cell.

In this paper, the boundary integral equations are discretized via a Nyström method but the fast direct solver can be applied the linear system arising from other discretizations. Let N_l denote the number of discretization points on interface Γ_l . As in [14], the quasi-periodicity is enforced at points that lie on Gaussian panels between each interface on the left and right walls of the unit cell. Let M_w denote the number of points used to enforce periodicity in a layer. (For simplicity of presentation, we assume this number is the same for all the layers.) Lastly, the continuity of the integral representation and the Rayleigh-Bloch expansions is enforced at collection of M uniformly distributed points on the top and bottom of the unit cell. The Rayleigh-Bloch expansions are truncated at $\pm K$.

The rectangular linear system that arises from these choices has the form

$$(2.17) \quad \begin{bmatrix} \mathbf{A} & \mathbf{B} & \mathbf{0} \\ \mathbf{C} & \mathbf{Q} & \mathbf{0} \\ \mathbf{Z} & \mathbf{V} & \mathbf{W} \end{bmatrix} \begin{bmatrix} \hat{\boldsymbol{\sigma}} \\ \mathbf{c} \\ \mathbf{a} \end{bmatrix} = \begin{bmatrix} \mathbf{f} \\ \mathbf{0} \\ \mathbf{0} \end{bmatrix}$$

where \mathbf{A} is a matrix of size $2N \times 2N$ where $N = \sum_{l=1}^I N_l$, \mathbf{B} is a matrix of size $2N \times P$ where $P = \sum_{l=1}^{I+1} P_l$, \mathbf{C} is a matrix of size $2(I+1)M_w \times N$, \mathbf{Q} is a matrix of size $2(I+1)M_w \times P$, \mathbf{Z} is a matrix of size $4M \times 2N$, \mathbf{V} is a matrix of size $4M \times P$, and \mathbf{W} is a matrix of size $4M \times 2(2K+1)$. The first row equation enforces the continuity of the scattered field and its flux through the interfaces. The second row equation enforces the quasi-periodicity of the solution and the flux. The last row equation enforces continuity of the integral representation and the Rayleigh-Bloch expansions.

When the interfaces geometries are complex, a large number of discretization points N are needed to achieve a desired accuracy. In this scenario, the cost of inverting a matrix the size of \mathbf{A} dominates the cost of building a direct solver. For this reason, it is best to build the direct solver in a manner that allows for the bulk of the computational cost associated with matrices of the size $2N \times 2N$ to be reused. To achieve this, we choose to build a fast

direct solver for (2.17) via the following block solve:

$$(2.18) \quad \hat{\boldsymbol{\sigma}} = -\mathbf{A}^{-1} \left([\mathbf{B} \ 0] \begin{bmatrix} \mathbf{c} \\ \mathbf{a} \end{bmatrix} + \mathbf{A}^{-1} \mathbf{f} \right)$$

$$(2.19) \quad \begin{bmatrix} \mathbf{c} \\ \mathbf{a} \end{bmatrix} = - \left(\begin{bmatrix} \mathbf{Q} & \mathbf{0} \\ \mathbf{V} & \mathbf{W} \end{bmatrix} - \begin{bmatrix} \mathbf{C} \\ \mathbf{Z} \end{bmatrix} \mathbf{A}^{-1} [\mathbf{B} \ 0] \right)^\dagger \begin{bmatrix} \mathbf{C} \\ \mathbf{Z} \end{bmatrix} \mathbf{A}^{-1} \mathbf{f}$$

where \dagger denotes the Penrose pseudo-inverse.

Each of the matrices (2.17) has a sparsity pattern that can be used to accelerate the block solve. The bulk of the acceleration will come from a fast direct solver for the matrix \mathbf{A} (see section 3.1).

The matrix \mathbf{A} is block tridiagonal matrix. The diagonal blocks of \mathbf{A} denoted \mathbf{A}_{ii} can be written as the sum of two matrices $\mathbf{A}_{s,ii}$ and $\mathbf{A}_{pm,ii}$ where $\mathbf{A}_{s,ii}$ corresponds to the integral operator on Γ_i in the unit cell evaluated on Γ_i , i.e.

$$\begin{bmatrix} -I + \left(D_{\Gamma_i, \Gamma_i}^{\omega_i} - D_{\Gamma_i, \Gamma_i}^{\omega_{i+1}} \right) & \left(S_{\Gamma_i, \Gamma_i}^{\omega_i} - S_{\Gamma_i, \Gamma_i}^{\omega_{i+1}} \right) \\ \left(T_{\Gamma_i, \Gamma_i}^{\omega_i} - T_{\Gamma_i, \Gamma_i}^{\omega_{i+1}} \right) & I + \left(D_{\Gamma_i, \Gamma_i}^{*, \omega_i} - D_{\Gamma_i, \Gamma_i}^{*, \omega_{i+1}} \right) \end{bmatrix},$$

where I denotes the identity operator, and $\mathbf{A}_{pm,ii}$ is the contributions from the left and right neighboring geometries, i.e.

$$\begin{bmatrix} \left(D_{\Gamma_i, \{pm, \Gamma_i\}}^{\omega_i} - D_{\Gamma_i, \{pm, \Gamma_i\}}^{\omega_{i+1}} \right) & \left(S_{\Gamma_i, \{pm, \Gamma_i\}}^{\omega_i} - S_{\Gamma_i, \{pm, \Gamma_i\}}^{\omega_{i+1}} \right) \\ \left(T_{\Gamma_i, \{pm, \Gamma_i\}}^{\omega_i} - T_{\Gamma_i, \{pm, \Gamma_i\}}^{\omega_{i+1}} \right) & \left(D_{\Gamma_i, \{pm, \Gamma_i\}}^{*, \omega_i} - D_{\Gamma_i, \{pm, \Gamma_i\}}^{*, \omega_{i+1}} \right) \end{bmatrix},$$

for $i = 1, \dots, I$. The upper diagonal block $\mathbf{A}_{i,i+1}$ corresponds to the integral operators on Γ_{i+1} being evaluated on Γ_i , i.e.

$$\begin{bmatrix} -\tilde{D}_{\Gamma_i, \Gamma_{i+1}}^{\omega_{i+1}} & -\tilde{S}_{\Gamma_i, \Gamma_{i+1}}^{\omega_{i+1}} \\ -\tilde{T}_{\Gamma_i, \Gamma_{i+1}}^{\omega_{i+1}} & -\tilde{D}_{\Gamma_i, \Gamma_{i+1}}^{*, \omega_{i+1}} \end{bmatrix},$$

for $i = 1, \dots, I-1$. The lower diagonal blocks $\mathbf{A}_{i,i-1}$ correspond to the integral operators on Γ_{i-1} being evaluated on Γ_i , i.e.

$$\begin{bmatrix} \tilde{D}_{\Gamma_i, \Gamma_{i-1}}^{\omega_i} & \tilde{S}_{\Gamma_i, \Gamma_{i-1}}^{\omega_i} \\ \tilde{T}_{\Gamma_i, \Gamma_{i-1}}^{\omega_i} & \tilde{D}_{\Gamma_i, \Gamma_{i-1}}^{*, \omega_i} \end{bmatrix},$$

for $i = 2, \dots, I$.

The matrix \mathbf{B} is upper block diagonal with block defines by

$$(2.20) \quad \mathbf{B}_{i,i} = \begin{bmatrix} \phi_1^{\omega_i} |_{\Gamma_i} & \cdots & \phi_P^{\omega_i} |_{\Gamma_i} \\ \frac{\partial \phi_1^{\omega_i}}{\partial \mathbf{n}} |_{\Gamma_i} & \cdots & \frac{\partial \phi_P^{\omega_i}}{\partial \mathbf{n}} |_{\Gamma_i} \end{bmatrix} \text{ and } \mathbf{B}_{i,i+1} = \begin{bmatrix} -\phi_1^{\omega_{i+1}} |_{\Gamma_i} & \cdots & -\phi_P^{\omega_{i+1}} |_{\Gamma_i} \\ -\frac{\partial \phi_1^{\omega_{i+1}}}{\partial \mathbf{n}} |_{\Gamma_i} & \cdots & -\frac{\partial \phi_P^{\omega_{i+1}}}{\partial \mathbf{n}} |_{\Gamma_i} \end{bmatrix}$$

for $i = 1, \dots, I$. The matrix \mathbf{C} is lower block diagonal with blocks define by

$$(2.21) \quad \mathbf{C}_{i,i} = \begin{bmatrix} \alpha^{-2} D_{R_i + \mathbf{d}, \Gamma_i}^{\omega_i} - \alpha D_{L_i - \mathbf{d}, \Gamma_i}^{\omega_i} & \alpha^{-2} S_{R_i + \mathbf{d}, \Gamma_i}^{\omega_i} - \alpha S_{L_i - \mathbf{d}, \Gamma_i}^{\omega_i} \\ \alpha^{-2} T_{R_i + \mathbf{d}, \Gamma_i}^{\omega_i} - \alpha T_{L_i - \mathbf{d}, \Gamma_i}^{\omega_i} & \alpha^{-2} D_{R_i + \mathbf{d}, \Gamma_i}^{*, \omega_i} - \alpha D_{L_i - \mathbf{d}, \Gamma_i}^{*, \omega_i} \end{bmatrix} \text{ and}$$

$$(2.22) \quad \mathbf{C}_{i,i-1} = \begin{bmatrix} \alpha^{-2} D_{R_i + \mathbf{d}, \Gamma_{i-1}}^{\omega_i} - \alpha D_{L_i - \mathbf{d}, \Gamma_{i-1}}^{\omega_i} & \alpha^{-2} S_{R_i + \mathbf{d}, \Gamma_{i-1}}^{\omega_i} - \alpha S_{L_i - \mathbf{d}, \Gamma_{i-1}}^{\omega_i} \\ \alpha^{-2} T_{R_i + \mathbf{d}, \Gamma_{i-1}}^{\omega_i} - \alpha T_{L_i - \mathbf{d}, \Gamma_{i-1}}^{\omega_i} & \alpha^{-2} D_{R_i + \mathbf{d}, \Gamma_{i-1}}^{*, \omega_i} - \alpha D_{L_i - \mathbf{d}, \Gamma_{i-1}}^{*, \omega_i} \end{bmatrix}$$

for $i = 1, \dots, I$ and $i = 2, \dots, I+1$, respectively. The matrix \mathbf{Q} is block diagonal with blocks given by

$$(2.23) \quad \mathbf{Q}_{ii} = \begin{bmatrix} \alpha^{-1} \phi_1^{\omega_i} |_{R_i} - \phi_1^{\omega_i} |_{L_i} & \cdots & \alpha^{-1} \phi_P^{\omega_i} |_{R_i} - \phi_P^{\omega_i} |_{L_i} \\ \alpha^{-1} \frac{\partial \phi_1^{\omega_i}}{\partial \mathbf{n}} |_{R_i} - \frac{\partial \phi_1^{\omega_i}}{\partial \mathbf{n}} |_{L_i} & \cdots & \alpha^{-1} \frac{\partial \phi_P^{\omega_i}}{\partial \mathbf{n}} |_{R_i} - \frac{\partial \phi_P^{\omega_i}}{\partial \mathbf{n}} |_{L_i} \end{bmatrix}$$

for $i = 1, \dots, I + 1$.

The matrices \mathbf{Z} , \mathbf{V} , and \mathbf{W} are sparse matrices of the form

$$\mathbf{Z} = \begin{bmatrix} \mathbf{Z}_U & \mathbf{0} & \cdots & \mathbf{0} \\ \mathbf{0} & \cdots & \mathbf{0} & \mathbf{Z}_D \end{bmatrix}, \quad \mathbf{V} = \begin{bmatrix} \mathbf{V}_U & \mathbf{0} & \cdots & \mathbf{0} \\ \mathbf{0} & \cdots & \mathbf{0} & \mathbf{V}_D \end{bmatrix}, \quad \text{and } \mathbf{W} = \begin{bmatrix} \mathbf{W}_U & \mathbf{0} \\ \mathbf{0} & \mathbf{W}_D \end{bmatrix}$$

where

$$(2.24) \quad \mathbf{Z}_U = \begin{bmatrix} \tilde{D}_{U,\Gamma_1}^{\omega_1} & \tilde{S}_{U,\Gamma_1}^{\omega_1} \\ \tilde{T}_{U,\Gamma_1}^{\omega_1} & \tilde{D}_{U,\Gamma_1}^{*,\omega_1} \end{bmatrix}, \quad \mathbf{Z}_D = \begin{bmatrix} \tilde{D}_{D,\Gamma_I}^{\omega_{I+1}} & \tilde{S}_{D,\Gamma_I}^{\omega_{I+1}} \\ \tilde{T}_{U,\Gamma_I}^{\omega_{I+1}} & \tilde{D}_{U,\Gamma_I}^{*,\omega_{I+1}} \end{bmatrix},$$

$$(2.25) \quad \mathbf{V}_U = \begin{bmatrix} \phi_1^{\omega_1}|_U & \cdots & \phi_P^{\omega_1}|_U \\ \frac{\phi_1^{\omega_1}}{\partial\nu}|_U & \cdots & \frac{\phi_P^{\omega_1}}{\partial\nu}|_U \end{bmatrix}, \quad \mathbf{V}_D = \begin{bmatrix} \phi_1^{\omega_{I+1}}|_D & \cdots & \phi_P^{\omega_{I+1}}|_D \\ \frac{\phi_1^{\omega_{I+1}}}{\partial\nu}|_D & \cdots & \frac{\phi_P^{\omega_{I+1}}}{\partial\nu}|_U \end{bmatrix},$$

$$(2.26) \quad \mathbf{W}_U = \begin{bmatrix} -e^{i\kappa-Kx}|_U & \cdots & -e^{i\kappa_K x}|_U \\ -ik_{-K}^U e^{i\kappa-Kx}|_U & \cdots & -ik_K^U e^{i\kappa_K x}|_U \end{bmatrix}, \quad \text{and } \mathbf{W}_D = \begin{bmatrix} -e^{i\kappa-Kx}|_D & \cdots & -e^{i\kappa_K x}|_D \\ ik_{-K}^D e^{i\kappa-Kx}|_D & \cdots & ik_K^D e^{i\kappa_K x}|_D \end{bmatrix}.$$

3. FAST DIRECT SOLVER

While exploiting the sparsity of the matrices can accelerate the construction of a direct solver, the speed gains are not sufficient for applications when the interface geometries are complex. The fast direct solver proposed in this section exploits not only sparsity but also the data sparse nature of the matrix \mathbf{A} .

The foundations of the fast direct solver is a fast inversion technique for the largest matrix in the system \mathbf{A} presented in section 3.1. The fast inversion of \mathbf{A} allows for $\hat{\boldsymbol{\sigma}}$ to be computed for a cost that scales linearly with N via equation (2.18). Constructing and applying the pseudo-inverse of the Schur complement

$$(3.1) \quad \mathbf{S} = - \left(\begin{bmatrix} \mathbf{Q} & \mathbf{0} \\ \mathbf{V} & \mathbf{W} \end{bmatrix} - \begin{bmatrix} \mathbf{C} \\ \mathbf{Z} \end{bmatrix} \mathbf{A}^{-1} [\mathbf{B} \quad \mathbf{0}] \right).$$

is needed to find \mathbf{c} and \mathbf{a} via (2.19). Since \mathbf{S} is ill-conditioned, we use an ϵ_{Schur} approximate singular value decomposition (SVD) to apply the pseudo-inverse.

Definition 3.1. Let $\mathbf{U}\boldsymbol{\Sigma}\mathbf{V}^*$ be the SVD of Schur complement matrix \mathbf{S} of size $(2(I+1)M_w + 4M) \times (P+2(2K+1))$ where $\boldsymbol{\Sigma}$ is a diagonal rectangular matrix with entries of the singular values of \mathbf{S} and matrices \mathbf{U} and \mathbf{V} are unitary matrices of size $(2(I+1)M_w + 4M) \times (2(I+1)M_w + 4M)$ and $(P+2(2K+1)) \times (P+2(2K+1))$, respectively. Then the ϵ_{Schur} approximate SVD is

$$\hat{\mathbf{U}}\hat{\boldsymbol{\Sigma}}\hat{\mathbf{V}}^*$$

where $\hat{\boldsymbol{\Sigma}}$ is a diagonal square matrix of size $l \times l$ where l is the number of singular values of \mathbf{S} that are larger than ϵ_{Schur} , $\hat{\mathbf{U}}$ is an $(2(I+1)M_w + 4M) \times l$ matrix and $\hat{\mathbf{V}}$ is an $(P+2(2K+1)) \times l$ matrix.

Then \mathbf{c} and \mathbf{a} can be approximated by

$$\begin{bmatrix} \mathbf{c} \\ \mathbf{a} \end{bmatrix} \approx \hat{\mathbf{V}}\hat{\boldsymbol{\Sigma}}^{-1}\hat{\mathbf{U}}^* \begin{bmatrix} \mathbf{C} \\ \mathbf{Z} \end{bmatrix} \mathbf{A}^{-1} \mathbf{f}.$$

Many of the components of the matrices in (2.17) can be re-used for multiple incident angles (i.e. all Bloch phases) as detailed in section 3.2. The combination of this and the fast direct solver for \mathbf{A} makes the fast direct solver ideal for problems where many solves are required. A key feature of the fast direct solver is that the bulk of the precomputation can be re-used if an interface Γ_j or a wave speed ω_j is changed. Section 3.3 details how this can be done.

3.1. Fast inversion of A. The key to building the fast direct solver for the block system (2.17) is having a fast way of inverting A. This technique is designed to make solves for different Bloch phases as efficient as possible.

The solver considers the matrix A written as the sum of two matrices

$$(3.2) \quad \mathbf{A} = \underbrace{\begin{bmatrix} A_{s,11} & 0 & 0 & 0 & 0 \\ 0 & A_{s,22} & 0 & 0 & 0 \\ 0 & 0 & \ddots & 0 & 0 \\ 0 & 0 & 0 & A_{s,(N-1)(N-1)} & 0 \\ 0 & 0 & 0 & 0 & A_{s,NN} \end{bmatrix}}_{\mathbf{A}_0} + \underbrace{\begin{bmatrix} A_{pm,11} & A_{12} & 0 & 0 & 0 \\ A_{21} & A_{pm,22} & A_{23} & 0 & 0 \\ 0 & 0 & \ddots & \ddots & 0 \\ 0 & 0 & A_{(N-1),(N-2)} & A_{pm,(N-1)(N-1)} & A_{(N-1),N} \\ 0 & 0 & 0 & A_{N,(N-1)} & A_{pm,NN} \end{bmatrix}}_{\hat{\mathbf{A}}}$$

where the block diagonal matrix \mathbf{A}_0 corresponds to the self-interaction and $\hat{\mathbf{A}}$ is the block tridiagonal matrix where the diagonal blocks correspond to the interaction of an interface with its left and right neighbors and the off-diagonal blocks correspond to the interactions between the interfaces directly above and below each other. Since the submatrices in $\hat{\mathbf{A}}$ correspond to “far” interactions, they are numerically low rank. Let LR denote the low rank factorization of $\hat{\mathbf{A}}$ where \mathbf{L} and \mathbf{R}^T are $2N \times k_{\text{tot}}$ matrices and k_{tot} is the numerical rank of $\hat{\mathbf{A}}$. Section 3.1.1 presents a technique for constructing this factorization. Then A can be approximated by

$$\mathbf{A} \sim \mathbf{A}_0 + \mathbf{LR}.$$

The advantage of this representation is that the factors \mathbf{L} and \mathbf{R} can be computed in a way that is independent of Bloch phase as presented in section 3.1.1. Additionally, the inverse can be formulated via a Woodbury formula [18]

$$(3.3) \quad \mathbf{A}^{-1} \sim (\mathbf{A}_0 + \mathbf{LR})^{-1} = \mathbf{A}_0^{-1} - \mathbf{A}_0^{-1}\mathbf{L}(\mathbf{I} + \mathbf{R}\mathbf{A}_0^{-1}\mathbf{L})^{-1}\mathbf{R}\mathbf{A}_0^{-1}.$$

Not only is the matrix \mathbf{A}_0 block diagonal but each of the diagonal blocks is amenable to a fast direct solver such as *Hierarchically Block Separable (HBS)* methods [17, 23, 10] which are closely related to the *Hierarchically Semi-Separable (HSS)* [41, 39, 40], the Hierarchical interpolative factorization [24], the \mathcal{H} and \mathcal{H}^2 -matrix methods [7, 8]. Thus \mathbf{A}_0 can be inverted and the inverse can be applied for a cost that scales linearly with the number of discretization points on the interfaces. This computation is independent of Bloch phase.

It is never necessary to construct the approximation of \mathbf{A}^{-1} . It is only necessary to have a fast algorithm for applying it to a vector $\mathbf{f} \in \mathbb{C}^{2N \times 1}$, i.e. a fast algorithm is needed for evaluating

$$(3.4) \quad \mathbf{A}^{-1}\mathbf{f} \sim \mathbf{A}_0^{-1}\mathbf{f} - \mathbf{A}_0^{-1}\mathbf{L}(\mathbf{I} + \mathbf{R}\mathbf{A}_0^{-1}\mathbf{L})^{-1}\mathbf{R}\mathbf{A}_0^{-1}\mathbf{f}.$$

The fast direct solver for \mathbf{A}_0 and the block structure of the matrices \mathbf{L} and \mathbf{R} allow for $\mathbf{A}_0^{-1}\mathbf{L}$ and $\mathbf{R}\mathbf{A}_0^{-1}\mathbf{f}$ to be evaluated for a cost that scales linearly with N . Thanks to the sparsity pattern of the matrices, the intermediate matrix $\mathbf{S}_2 = \mathbf{I} + \mathbf{R}\mathbf{A}_0^{-1}\mathbf{L}$ of size $k_{\text{tot}} \times k_{\text{tot}}$ that needs to be inverted is block tridiagonal. Appendix A reports on the construction of \mathbf{S}_2 . Since k_{tot} is much smaller than N in practice, the inverse of \mathbf{S}_2 can be applied rapidly using

a block variant of the Thomas algorithm. This computation needs to be done for each new Bloch phase since L and R are dependent on Bloch phase.

Remark 3.1. To achieve nearly optimal ranks in the construction of the fast direct solver, it is advantageous to reorder the matrices in A according to the physical location of the unknowns. For example, if there are N_1 discretization points on Γ_1 , the unknowns are $\sigma_{1,1}, \dots, \sigma_{1,N_1}$ and $\tau_{1,1}, \dots, \tau_{1,N_1}$, etc. Then the matrices should be ordered so $\hat{\sigma}$ is as follows

$$\hat{\sigma}^T = [\sigma_{1,1}, \tau_{1,1}, \dots, \sigma_{1,N_1}, \tau_{1,N_1}, \dots, \sigma_{I,1}, \tau_{I,1}, \dots, \sigma_{I,N_I}, \tau_{I,N_I}].$$

3.1.1. *Low rank factorization of \hat{A} .* The technique for creating the low rank factorizations of the blocks of in \hat{A} is slightly different depending on whether or not the block is diagonal. This section begins by presenting the technique for creating low rank factorizations of the diagonal blocks. Then the technique for creating the low rank factorization of the off-diagonal blocks is presented.

Recall the diagonal blocks of \hat{A} are $A_{pm,ii}$ correspond to the discretized version of

$$(\mathcal{S}_{\Gamma_i, \{pm, \Gamma_i\}}^\omega \rho)(\mathbf{x}) = \underbrace{\alpha \int_{\Gamma_i} G_\omega(\mathbf{x}, \mathbf{y} + \mathbf{d}) \rho(\mathbf{y}) dl(\mathbf{y})}_{\text{right copy: } (\mathcal{S}_{\Gamma_i, \{p, \Gamma_i\}}^\omega \rho)(\mathbf{x})} + \alpha^{-1} \underbrace{\int_{\Gamma_i} G_\omega(\mathbf{x}, \mathbf{y} - \mathbf{d}) \rho(\mathbf{y}) dl(\mathbf{y})}_{\text{left copy: } (\mathcal{S}_{\Gamma_i, \{m, \Gamma_i\}}^\omega \rho)(\mathbf{x})}.$$

This means that the matrix can be written as two parts that are independent of Bloch phase. Specifically, $A_{pm,ii} = \alpha A_{p,ii} + \alpha^{-1} A_{m,ii}$. Thus by creating low rank factorizations of $A_{p,ii}$ and $A_{m,ii}$ independently, the factorizations can be used for any Bloch phase α . Let $L_{i,p} R_{i,p}$ and $L_{i,m} R_{i,m}$ denote the low rank approximations of $A_{p,ii}$ and $A_{m,ii}$ respectively. These two approximations are combined to create a low rank approximation of $A_{pm,ii}$ as follows:

$$A_{pm,ii} \approx \underbrace{\begin{bmatrix} L_{i,p} & L_{i,m} \end{bmatrix}}_{L_{pm,ii}} \underbrace{\begin{bmatrix} \alpha R_{i,p} \\ \alpha^{-1} R_{i,m} \end{bmatrix}}_{R_{pm,ii}}$$

The technique is similar to the one used in [33] to create low rank factorizations of $A_{m,ii}$ and $A_{p,ii}$ but has an extra step to keep k_{tot} small.

For brevity, the technique for compressing the interaction with the left neighbor (i.e. computing the low rank factorization of $A_{m,ii}$) is presented. The technique for compressing the interaction with the right neighbor follows directly.

We choose to build the factorization via the interpolatory decomposition [20, 12] defined as follows.

Definition 3.2. The *interpolatory decomposition* of a $m \times n$ matrix M that has rank l is the factorization

$$M = PM(J(1:l), :)$$

where J is a vector of integers j such $1 \leq j \leq m$, and P is a $m \times l$ matrix that contains a $l \times l$ identity matrix. Namely, $P(J(1:l), :) = I_l$.

Creating the low rank factorization of $A_{m,ii}$ by directly plugging it into the interpolatory decomposition has a computational cost of $O(N_i^2 k_i)$ where k_i is the numerical rank of $A_{m,ii}$. This would result in a solution technique that has a computational cost that scales quadratically, *not linearly*, with respect to N . To restore the linear computational complexity, we utilize potential theory.

Recall Γ_i denotes the part of the i^{th} interface in the unit cell. Let $\Gamma_{m,i}$ denote the part of the i^{th} interface in the left neighboring cell. First Γ_i is partitioned into a collection of S

segments γ_j via dyadic refinement where the segments get smaller as they approach $\Gamma_{m,i}$ so that $\Gamma_i = \cup_{j=1}^S \gamma_j$. Figure 3.1 illustrates a partitioning when compressing the interaction with $\Gamma_{m,i}$. The refinement is stopped when the segment closest to $\Gamma_{m,i}$ has less than n_{\max} points on it. Typically, $n_{\max} = 45$ is a good choice.

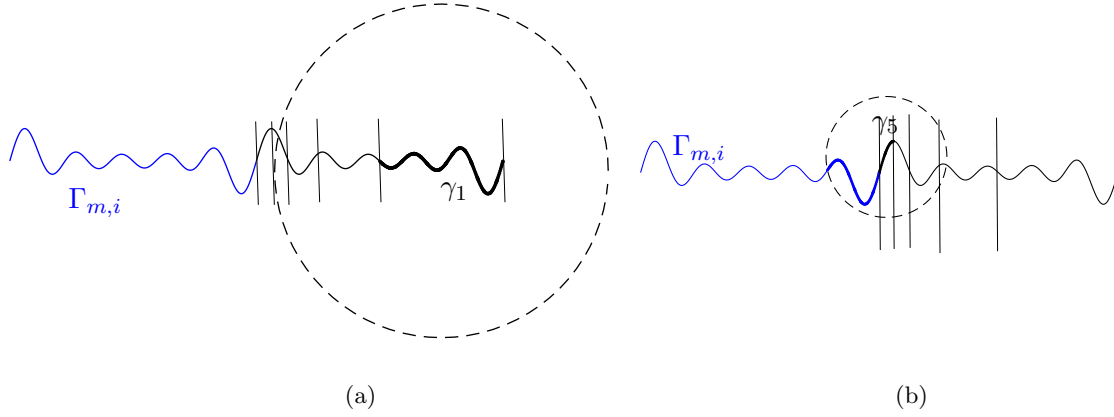


FIGURE 3.1. Illustration of the dyadic refinement partitioning of Γ_i with 5 levels of refinement and geometries for compressing $\mathbf{A}_{m,ii}$. (a) Illustration of the proxy surface (dashed circle) used to compress neighbor interactions when γ_l is far. (c) Illustration of the proxy surface (dashed circle) and near points (bold blue curve on $\Gamma_{m,i}$) when γ_l is touching $\Gamma_{m,i}$.

For each segment γ_j not touching $\Gamma_{m,i}$, consider a circle concentric with the bounding box containing γ_j with a radius slightly less than the distance from the center of the bounding box and $\Gamma_{m,i}$. Figure 3.1(a) illustrates the proxy surface for γ_1 when there is 5 levels of dyadic refinement toward $\Gamma_{m,i}$. From potential theory, we know that any field generated by sources outside of this circle can be approximated to high accuracy by placing enough equivalent charges on the circle. In practice, it is enough to place a small number of *proxy points* evenly on the circle. Let n_{proxy} denote the number of proxy points on the circle. For problems where the direct solver scales linearly, n_{proxy} is small and chosen to be a constant independent of ω_i . For the experiments in this paper, it is sufficient to have $n_{\text{proxy}} = 80$. Let n_j denote the number of points on γ_j . An interpolatory decomposition can be constructed for the matrix $\mathbf{A}^{\text{proxy}}$ capturing the interaction between γ_j and the proxy points. The result is an index vector J_j and an interpolation matrix \mathbf{P}_j of size $n_j \times k_j$ where k_j is the numerical rank of $\mathbf{A}^{\text{proxy}}$. For γ_S (the segment touching $\Gamma_{m,i}$), n_{proxy} proxy points are placed uniformly on a circle of radius 1.75 the smallest circle containing all the points on γ_S . All the points on $\Gamma_{m,i}$ inside the circle are labeled *near points* and indexed I_{near} . Figure 3.1(b) illustrates the proxy circle and near points for γ_5 when there is 5 levels of dyadic refine toward $\Gamma_{m,i}$. An interpolatory decomposition is then performed on $[\mathbf{A}_{m,ii}(\gamma_S, I_{\text{near}}) \mid \mathbf{A}^{\text{proxy}}]$. The result is an index vector J_S and an interpolation matrix \mathbf{P}_S of size $n_S \times k_S$.

The low rank factorization of the matrix $\mathbf{A}_{m,ii}$ can be constructed with the result of this compression procedure. Let $J = [J_1(1 : k_1), \dots, J_S(1 : k_S)]$ denote an index vector. Then $\mathbf{L}_{m,i}$ is a block diagonal matrix with block entries \mathbf{P}_j for $J = 1, \dots, S$ and $\mathbf{R}_{m,i} = \mathbf{A}_{m,ii}(J, :)$. The index vector J has a physical meaning. Specifically, the points on Γ_i corresponding to the index vector J are called the *skeleton points*.

This factorization is far from optimal rank and will result in a much larger than necessary constant prefactor in the application of the Woodbury formula (3.3). Thus a recompression

step is necessary. Let k_{orig} denote the rank of the original approximate factorization, i.e. the length of J . If k_{orig} is small enough, applying the interpolatory decomposition to $\mathbf{A}_{m,ii}(J, :)$ can be done efficiently. An index vector J_{up} and interpolation matrix \mathbf{P}_{up} of size $k_{\text{orig}} \times k_{\text{up}}$. Let $\mathbf{L}_{\text{up}} = \mathbf{P}_{\text{up}}$. Otherwise, the interpolatory decomposition can be applied to the submatrices corresponding to a lump of the segments at time. For example, suppose S is even, then the segments can be bunched two at a time. The interpolatory decomposition can be applied to $\mathbf{A}_{m,ii}([J_j(1 : k_j), J_{j+1}(1 : k_{j+1})], :)$ for $j = 1, \dots, S/2$. The resulting interpolation matrices are the block diagonal entries for the block diagonal matrix \mathbf{L}_{up} . The corresponding index vector J_{up} is formed in a similar manner to the vector J . Finally the low rank factorization of $\mathbf{A}_{m,ii}$ can be formed by multiplying $\mathbf{L}_{m,i}$ from before by \mathbf{L}_{up} and using the updated skeleton of $J(J_{\text{up}})$. In other words, $\mathbf{L}_{m,i} = \mathbf{L}_{m,i}\mathbf{L}_{\text{up}}$ and $\mathbf{R}_{m,i} = \mathbf{A}_{ii,m}(J(J_{\text{up}}), :)$.

The technique for constructing the low rank factorization of the off-diagonal blocks of $\hat{\mathbf{A}}$ is similar. Recall that each off-diagonal block \mathbf{A}_{ij} , for $i \neq j$, corresponds to the discretization of the following integral operator where $\mathbf{x} \in \Gamma_i$:

$$\begin{aligned} (\tilde{\mathcal{S}}_{\Gamma_i, \{\Gamma_j\}}^\omega \rho)(\mathbf{x}) &= \int_{\Gamma_j} G_\omega(\mathbf{x}, \mathbf{y}) \rho(\mathbf{y}) d\mathbf{l}(\mathbf{y}) + \alpha \int_{\Gamma_j} G_\omega(\mathbf{x}, \mathbf{y} + \mathbf{d}) \rho(\mathbf{y}) d\mathbf{l}(\mathbf{y}) \\ &\quad + \alpha^{-1} \int_{\Gamma_j} G_\omega(\mathbf{x}, \mathbf{y} - \mathbf{d}) \rho(\mathbf{y}) d\mathbf{l}(\mathbf{y}). \end{aligned}$$

It is natural to write \mathbf{A}_{ij} as the summation of three parts,

$$\mathbf{A}_{ij} = \mathbf{A}_{0,ij} + \alpha \mathbf{A}_{p,ij} + \alpha^{-1} \mathbf{A}_{m,ij},$$

where $\mathbf{A}_{0,ij}$, $\mathbf{A}_{p,ij}$, and $\mathbf{A}_{m,ij}$ are the discrete approximations of the corresponding integral operators.

While the actual matrix entries of $\mathbf{A}_{i,j}$ are dependent on α , the low rank factorization can be computed independent of α since we are using the interpolatory decomposition. As with the diagonal blocks, building the factorization of \mathbf{A}_{ij} directly is computationally prohibitive. (The computational cost of the direct factorization is $O(N_i N_j k_{ij})$ where k_{ij} is the numerical rank of \mathbf{A}_{ij} .) Potential theory is again utilized to decrease the computational cost. Consider an ellipse horizontally large enough to enclose Γ_i and vertically shields Γ_i from its top and bottom neighbor interface. A collection of n_{proxy} equivalent charges are evenly distributed on the ellipse in parameter space. Figure 3.2 illustrates a proxy surface used for compressing $\mathbf{A}_{i,i+1}$. The interpolatory decomposition is applied to the matrix characterizing the interactions between the points on Γ_i and the proxy surface, $\mathbf{A}^{\text{proxy}}$. The index vector J_i and the $N_i \times k_{\text{proxy}}$ interpolation matrix $\mathbf{P}_{1,ij}$ are returned. Let $J_1 = J_i(1 : k_{\text{proxy}})$.

As with the diagonal block factorization, k_{proxy} is far from the optimal rank. To reduce the rank, we apply the interpolatory decomposition to $[\mathbf{A}_{0,ij} | \mathbf{A}_{p,ij} | \mathbf{A}_{m,ij}](J_1, :)$. An $k_{\text{proxy}} \times k_{\text{new}}$ interpolation matrix $\mathbf{P}_{\text{new},ij}$ and index vector J_{new} are returned. Then low rank factorization is complete. One factor can be used for all Bloch phases; $\mathbf{L}_{ij} = \mathbf{P}_{1,ij} \mathbf{P}_{\text{new},ij}$. The other factor is simply a matrix evaluation; $\mathbf{R}_{ij} = \mathbf{A}_{ij}(J_{ij}, :)$ where $J_{ij} = J_1(J_{\text{new}})$. It is important to note that the matrices $\mathbf{A}_{0,ij}(J_{ij}, :)$, $\mathbf{A}_{p,ij}(J_{ij}, :)$ and $\mathbf{A}_{m,ij}(J_{ij}, :)$ are computed once as they are independent of Bloch phase. Thus constructing \mathbf{R}_{ij} is simply matrix addition for each new Bloch phase.

3.2. The Bloch phase and incident angle dependence. Beyond the matrix \mathbf{A} and exploiting the sparsity of the other matrices in (2.17), additional acceleration can be gained for problems where the solution is desired for multiple incident angles.

The matrix \mathbf{B} has entries (2.20) that are independent of Bloch phase and thus need only be computed once. This is also the case for \mathbf{V} . The non-zero block matrices in \mathbf{C} are (2.21)

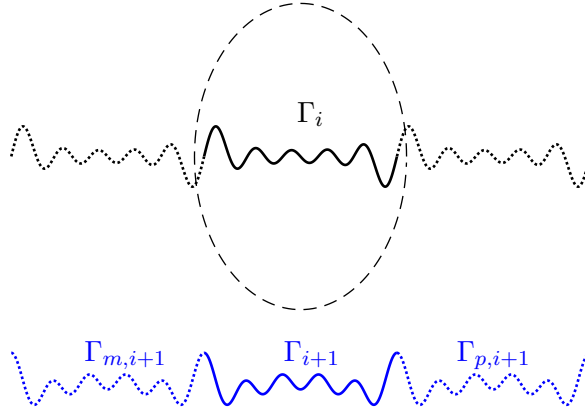


FIGURE 3.2. Illustration of the proxy surface for compressing $A_{i,i+1}$.

and (2.22) dependent on α but only as a constant multiple. Thus the submatrices of C can be precomputed and used for all incident angles. The same statement is true for Q , and Z .

The only matrix that has entries that are dependent on incident angle is W . In fact, W is only dependent on Bloch phase α . Recall that for the Bloch phase $\alpha = e^{id\omega_1 \cos \theta^{\text{inc}}}$. This means that for all incident angles that share a Bloch phase, there exist a representative angle $\hat{\theta}$ such that $\omega_1 \cos \theta^{\text{inc}} = \hat{\theta} + \frac{2\pi m}{d}$ for $m \in \mathbb{Z}$. Since the entries of W involve

$$e^{i\kappa_j x} = e^{i(\omega_1 \cos \theta^{\text{inc}} + \frac{2\pi j}{d})x}$$

for $j = -K, \dots, K$. Thus the entries of W are off by a shift in index for incident angles that share a Bloch phase. Thus it is possible to construct W so that it can be used for all angles that share a Bloch phase. Suppose that we know that 12 incident angles $\{\theta_1^{\text{inc}}, \dots, \theta_{12}^{\text{inc}}\}$ share a Bloch phase and $\omega_1 \cos \theta_j^{\text{inc}} = \hat{\theta} + \frac{2\pi(j-1)}{d}$ for $j = 1, \dots, 12$. Then we construct W so that it has entries with κ_j indexed from $-K$ to $K + 12$. By doing this, we also get to re-use the SVD of S for all angles that have a shared Bloch phase. This is substantial savings in the shared Bloch phase solves. To evaluate the solution using the resulting coefficients for the Rayleigh-Bloch expansion above or below the unit cell, it is only necessary to use the terms that correspond to $-K, \dots, K$ for that incident angle.

3.3. Extensions. Many applications consider the boundary value problem (1.1) for a collection of geometries where the variation is in a single interface or the wave speed in a layer. The proposed direct solver can efficiently update an existing fast direct solver for these localized changes in the geometry.

For example, if a user wants to replace Γ_i , the parts of the direct solver for A corresponding to that block row and column need to be recomputed. The corresponding block columns of C and corresponding block rows of B also need to be recomputed. If the replaced layer is either the top or the bottom, then subblocks in V and Z need to be updated as well. Independent of the interface changed, the cost of creating a new direct solver is linear with respect to the number of discretization points on the new interface.

If a user wants to change the wave number ω_i in Ω_i where $1 < i < I$, there are two interfaces affected Γ_i and Γ_{i+1} . The corresponding blocks rows and columns of the fast direct solver of A need to be recomputed. In addition to updating those matrices, the corresponding

blocks in \mathbf{B} , \mathbf{C} and \mathbf{Q} need to be updated. If the wave number is changed in the top or bottom layer, then the corresponding blocks in \mathbf{Z} and \mathbf{V} need to be updated as well. Again the cost of updating the direct solver scales linearly with number of discretization points on the interfaces affected $N_i + N_{i+1}$.

4. NUMERICAL EXAMPLES

This section illustrates the performance of the fast direct solver for several eleven layered geometries. This is simply for presentation purposes. The solution technique can be applied to geometries of arbitrary number of layers. Section 4.1 demonstrates the scaling of the fast direct solver for the eleven layer geometry illustrated in Figure 4.1 where the wave number alternates between 40 and $40\sqrt{2}$ in the layers. The ability for the solution technique to solve (1.1) for hundreds of incident waves is reported. Section 4.3 illustrates the performance of the solution technique for two changes in the problem (1.1): (i) an interface geometry is changed and (ii) a wave number is changed in one of the layers.

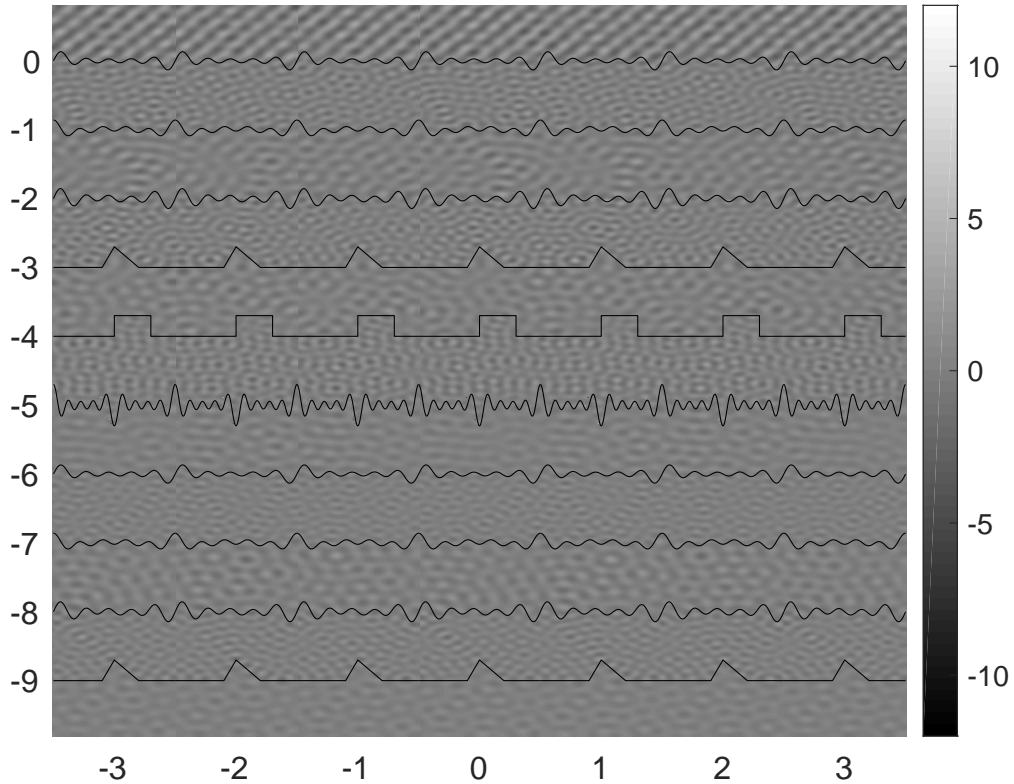


FIGURE 4.1. Illustration of the real part of the total field of the solution to (1.1) for a geometry with 10 interfaces where the wave number alternates between 40 and $40\sqrt{2}$ and the incident angle is fixed at $\theta^{inc} = -\frac{\pi}{5}$. The total number of discretization points was set to $N = 52160$, resulting in a flux error estimate of $3.44e - 09$. Seven periods in the geometry are shown.

The test geometries have period fixed at $d = 1$, and the vertical separation between the neighbor interfaces is roughly 1. The interfaces are discretized via the Nyström method

with a 16-point Gaussian quadrature. The diagonal blocks require specialized quadrature to handle the weakly singular kernels. We chose to use generalized Gaussian [21] quadrature. The fast direct solver is compatible with other specialized quadrature for the diagonal blocks such as that of Alpert [2], that of Helsing [22], Kapur–Rokhlin rule [27], or QBX [29]. The corresponding base quadrature should be adjusted if needed. Interfaces that are smooth and have corners are considered. Interfaces with sharp corners are discretized with three-levels dyadic refinement into each corner and the integral operators are discretized in \mathcal{L}^2 [9]. The artificial separation walls and proxy circles are discretized with the similar parameter choices as in [14]: the left and right (vertical) artificial walls for each layer are discretized by $M_w = 120$ nodes Gauss-Legendre quadrature; $M = 60$ equispaced nodes are sampled from the (horizontal) upper and lower wall; $P = 160$ equispaced nodes are chosen on the proxy circle for each layer. For the wave number under consideration in these experiments, it is sufficient to truncate the Rayleigh-Bloch expansions at $K = 20$.

For all experiments, an HBS fast direct solver with tolerance $\epsilon = 10^{-12}$ was used to construct the approximation of \mathbf{A}_0^{-1} in (3.3). The tolerance for all other low rank factorizations was also set to 10^{-12} . The SVD of \mathbf{S} was truncated at $\epsilon_{\text{Schur}} = 10^{-13}$.

All experiments were run on a dual 2.3 GHz Intel Xeon Processor E5-2695 v3 desktop workstation with 256 GB of RAM. The code was implemented in MATLAB, apart from the evaluation of Hankel functions in the kernel evaluation and the interpolatory decomposition, which use Fortran.

The computational cost of the direct solution technique can be broken into 4 parts:

- Precomputation I: This includes the development of all fast linear algebra for applying the approximate \mathbf{A}^{-1} as presented in section 3.1. All factors are stored in their Bloch phase independent form.
- Precomputation II: This is the remainder of the precomputation that is independent of Bloch phase as presented in section 3.2.
- Precomputation III: This is the all precomputation that can be used for all incident angles that share a Bloch phase α , including scaling matrices by α , construction of the matrix \mathbf{W} as explained in section 3.2, constructing the fast apply of \mathbf{A}^{-1} , evaluating the Schur complement matrix \mathbf{S} (3.1), and computing the ϵ_{Schur} SVD of \mathbf{S} .
- Solve: This is the application of the precomputed solver to the right hand side of (2.17) via (2.18) and (2.19).

The error is approximated via an flux error estimate as in [14]. This has been demonstrated to agree very well with the relative error at any point in the domain so no other errors are reported.

4.1. Scaling experiment. This section illustrates the scaling of the fast direct solver for the geometry illustrated in figure 4.1.

In the first experiment, the wave number in the layers remains fixed (alternating between 40 and $40\sqrt{2}$) while the number of discretization points per layer increases. Table 1 reports the time in seconds for each part of the direct solver. For this geometry, the solution technique achieves a relative flux error of $3.37e - 09$ when $N = 26560$. Each part of the solution technique scales linearly with respect to N . As expected the precomputation dominates the cost of the solver. Precomputation parts I, II and III use approximately 85%, 4%, and 10%, respectively, of the precomputation time. Thus the parts of the solver that are independent of Bloch phase dominate the computational cost.

4.2. Sweep over multiple incident angles. Many applications require solving (1.1) for many incident angles (as discussed in section 1). In this setting, precomputation parts I and

N	Precomp I	Precomp II	Precomp III	Solve
7360	88.13	4.15	10.70	0.40
13728	162.99	6.81	16.86	1.05
26560	303.66	13.18	29.79	1.85
52160	557.08	24.01	56.16	2.83
103360	1043.31	48.53	109.65	6.35
205760	2026.78	103.01	220.41	14.22

TABLE 1. Time in seconds for applying the direct solver to an 11-layer test geometry with N discretization points on the interfaces.

N	Precomp I	Precomp II	Precomp III	Solve
52160	554.01	25.07	1411.35 (58.81 per Bloch phase)	118.35 (0.41 per incident angle)

TABLE 2. Run time in seconds for solving 287 incident angles and 24 distinct Bloch phases on an 11-layer geometry. The incident angles are sampled from $[-0.89\pi, -0.11\pi]$. The geometry is discretized with $N = 52160$.

II need only be done once. Precomputation part III can be utilized for all incident angles that share a Bloch phase α . Table 2 reports the time in seconds for all parts of the solution technique when applied to (1.1) on the geometry illustrated in figure 4.1 with the wave number alternating between 40 and $40\sqrt{2}$ for 287 incident angles between $[-0.89\pi, -0.11\pi]$ corresponding to 24 different Bloch phases. The total number of discretization points on the interface is fixed at $N = 52160$ resulting in flux errors of roughly $1e - 8$ to $1e - 10$ for all of the chosen angles. Since the first two parts of the precomputation dominate the computational cost, significant speed up over building the direct solver for each angle independently is observed. For this problem, exploiting the ability to reuse computations for share Bloch phase results in a 87 times faster than building a fast direct solver from scratch for each incident angle.

4.3. Local change to the geometry. This section illustrates the performance of the direct solver when there is a change in one layer of the geometry for the boundary value problem. Either a change in an interface or the wave number in a layer.

We consider the eleven layer problem where the wave number alternates between 40 and $40\sqrt{2}$ to be the original problem. The timing in seconds for each part of the direct solver for the original geometry are reported in Table 1. In the first experiment, the fourth interface in this geometry is changed. Figure 4.2 illustrates the original and new geometries. In the second experiment, the wave number for the second layer is changed from $40\sqrt{2}$ to 30. As presented in section 3.2, only a small number of the matrices in each step of the precomputation need to be recomputed. Table 3 reports the time in seconds for updating the direct solver made for the original geometry to solve the problems on the new geometries. The precomputation parts I and II are roughly 8 times faster than computing these from scratch for the new geometry. Since the change in the wave speed has an impact on two interfaces, the update is more expensive than the update for the change in interface as expected. Independent, when an application requires many solves per new geometry and many new geometries need to be considered, the speed gains over building a solver from scratch for each new geometry will be significant.

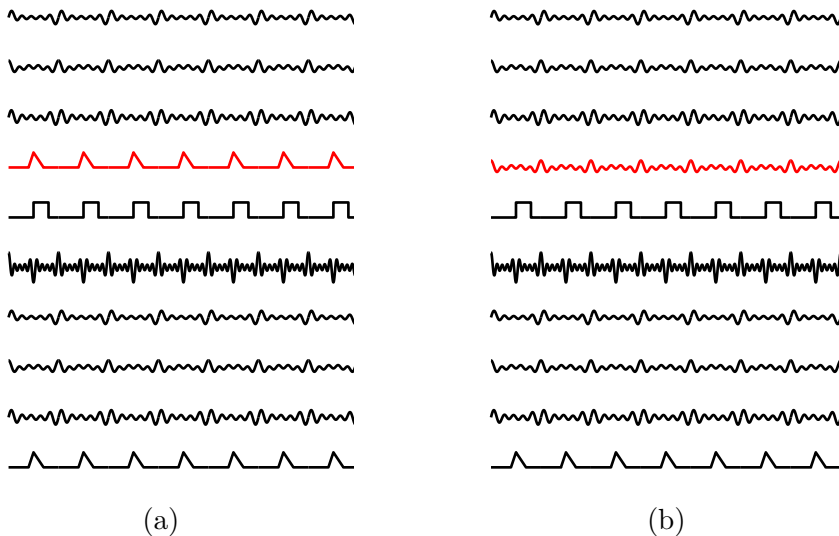


FIGURE 4.2. Illustration of (a) the original 11-layer structure and (b) the new structure obtained from replacing the fourth interface with a different geometry. The interface that is changed is plotted in red. Seven periods of both geometries are shown.

	Replace interface Γ_4	Change wave number $\omega_2 = 30$
N	51824	52160
Precomp I	56.60	88.80
Precomp II	10.77	2.42
Precomp III	41.68	37.39
Solve	2.40	1.54

TABLE 3. Time in seconds for constructing and applying the fast direct solver for a geometry that has the fourth interface change (first column) and the wave number for the second layer changed from $40\sqrt{2}$ to 30. N is the number of discretization points on the interfaces in the unit cell.

5. CONCLUSION

This paper presented a fast direct solution technique for multilayered medium quasi-periodic scattering problem. For low frequency problems, the computational cost of the direct solver scales linearly with the number of discretization points. The bulk of the precomputation can be used for all solves independent of incident angle and Bloch phase α . In the example in section 4.2 involving an eleven geometry discretized with 52160 unknowns, 287 incident angles are solved in under 8 seconds per angle.

An additional benefit of this solution technique is that modifications in a wave number in layer or an interface result in only having to update the matrices corresponding to that layer or interface. The cost of updating the precomputation parts scales linearly with the number of points on that interface. For optimal design and inverse scattering applications

where the geometry will be changed many times and for each geometry many solves are required, the fast direct solver will have significant savings.

The extension to three dimensional problems is not trivial but the work presented in this paper provides the foundations for that work.

6. ACKNOWLEDGEMENTS

The work of A. Gillman is supported by the National Science Foundation (DMS-1522631).

REFERENCES

- [1] M. Abramowitz and I. Stegun, editors. *Handbook of Mathematical Functions*. Dover, New York, 1964.
- [2] B. Alpert. Hybrid gauss-trapezoidal quadrature rules. *SIAM Journal on Scientific Computing*, 20(5):1551–1584, 1999.
- [3] H. A. Atwater and A. Polman. Plasmonics for improved photovoltaic devices. *Nature Materials*, 9:205–213, 2010.
- [4] I. M. Babuska and S. A. Sauter. Is the pollution effect of the FEM avoidable for the Helmholtz equation considering high wave numbers? *SIAM Journal of Numerical Analysis*, 34(6):2392–2423, 1997.
- [5] A. Barnett and L. Greengard. A new integral representation for quasi-periodic fields and its application to two-dimensional band structure calculations. *Journal of Computational Physics*, 229:6898–6914, 2010.
- [6] C. Barty, M. Key, J. Britten, R. Beach, G. Beer, C. Brown, S. Bryan, J. Caird, T. Carlson, J. Crane, J. Dawson, A. Erlandson, D. Fittinghoff, M. Hermann, C. Hoaglan, A. Iyer, L. J. II, I. Jovanovic, A. Komashko, O. Landen, Z. Liao, W. Molander, S. Mitchell, E. Moses, N. Nielsen, H.-H. Nguyen, J. Nissen, S. Payne, D. Pennington, L. Risinger, M. Rushford, K. Skulina, M. Spaeth, B. Stuart, G. Tietbohl, and B. Wattellier. An overview of llnl high-energy short-pulse technology for advanced radiography of laser fusion experiments. *Nuclear Fusion*, 44(12):S266, 2004.
- [7] S. Börm. *Efficient numerical methods for non-local operators*, volume 14 of *EMS Tracts in Mathematics*. European Mathematical Society (EMS), Zürich, 2010.
- [8] S. Börm and W. Hackbusch. Approximation of boundary element operators by adaptive \mathcal{H}^2 -matrices. In *Foundations of computational mathematics: Minneapolis, 2002*, volume 312 of *London Math. Soc. Lecture Note Ser.*, pages 58–75. Cambridge Univ. Press, Cambridge, 2004.
- [9] J. Bremer. On the Nyström discretization of integral operators on planar domains with corners. *Applied and Computational Harmonic Analysis*, 32:45–64, 2012.
- [10] J. Bremer, A. Gillman, and P. Martinsson. A high-order accurate accelerated direct solver for acoustic scattering from surfaces. *BIT Numerical Mathematics*, 55:141–170, 2015.
- [11] O. P. Bruno and A. G. Fernandez-Lado. Rapidly convergent quasi-periodic green functions for scattering by arrays of cylinders—including wood anomalies. *Proceedings of the Royal Society of London A: Mathematical, Physical and Engineering Sciences*, 473(2199), 2017.
- [12] H. Cheng, Z. Gimbutas, P. Martinsson, and V. Rokhlin. On the compression of low rank matrices. *SIAM Journal of Scientific Computing*, 26(4):1389–1404, 2005.
- [13] M. Cho. Spectrally-accurate numerical method for acoustic scattering from doubly-periodic 3d multi-layered media, 2018. arXiv:1806.03813.
- [14] M. Cho and A. Barnett. Robust fast direct integral equation solver for quasi-periodic scattering problems with a large number of layers. *Optics Express*, 23(2):1775–1799, 2015.
- [15] D. Colton and R. Kress. *Inverse acoustic and electromagnetic scattering theory*, volume 93 of *Applied Mathematical Sciences*. Springer-Verlag, Berlin, second edition, 1998.
- [16] C. Geuzaine and J.-F. Remacle. Gmsh: a three-dimensional finite element mesh generator with built-in pre- and post-processing facilities. *International Journal for Numerical Methods in Engineering*, 79(11):1309–1331, 2009.
- [17] A. Gillman, P. Young, and P. Martinsson. A direct solver $O(N)$ complexity for integral equations on one-dimensional domains. *Frontiers of Mathematics in China*, 7:217–247, 2012.
- [18] G. H. Golub and C. F. Van Loan. *Matrix computations*. Johns Hopkins Studies in the Mathematical Sciences. Johns Hopkins University Press, Baltimore, MD, third edition, 1996.
- [19] L. Greengard, K. Ho, and J.-Y. Lee. A fast direct solver for scattering from periodic structures with multiple material interfaces in two dimensions. *J. Comput. Phys.*, 258:738–751., 2014.
- [20] M. Gu and S. C. Eisenstat. Efficient algorithms for computing a strong rank-revealing QR factorization. *SIAM Journal on Scientific Computing*, 17(4):848–869, 1996.

- [21] S. Hao, A. H. Barnett, P. G. Martinsson, and P. Young. High-order accurate nystrom discretization of integral equations with weakly singular kernels on smooth curves in the plane. *Advances in Computational Mathematics*, 40:245–272, 2013.
- [22] J. Helsing and R. Ojala. Corner singularities for elliptic problems: integral equations, graded meshes, quadrature, and compressed inverse preconditioning. *Journal of Computational Physics*, 227:8820–8840, 2008.
- [23] K. Ho and L. Greengard. A fast direct solver for structured linear systems by recursive skeletonization. *SIAM Journal of Scientific Computing*, 34(5):2507–2532, 2012.
- [24] K. Ho and L. Ying. Hierarchical interpolative factorization for elliptic operators: Integral equations. *Communications on Pure and Applied Mathematics*, 69(7):1314–1353, 2015.
- [25] T. Hughes. *The Finite Element Method: Linear Static and Dynamic Finite Element Analysis*. Dover Publications, 2000.
- [26] G. A. Kalinchenko and A. M. Lerer. Wideband all-dielectric diffraction grating on chirped mirror. *Journal of Lightwave Technology*, 28:2743–2749, 2010.
- [27] S. Kapur and V. Rokhlin. High-order corrected trapezoidal quadrature rules for singular functions. *SIAM Journal of Numerical Analysis*, 34(4):1331–1356, 1997.
- [28] M. D. Kelzenberg, S. W. Boettcher, J. A. Petykiewicz, D. B. Turner-Evans, M. C. Putnam, E. L. Warren, J. M. Spurgeon, R. M. Briggs, N. S. Lewis, and H. A. Atwater. Enhanced absorption and carrier collection in si wire arrays for photovoltaic applications. *Nature Materials*, 9:239–244, 2010.
- [29] A. Klöckner, A. Barnett, L. Greengard, and M. O’Neil. Quadrature by expansion: A new method for the evaluation of layer potentials. *Journal of Computational Physics*, 252:332 – 349, 2013.
- [30] D. Komatitsch and J. Tromp. A perfectly matched layer absorbing boundary condition for the second-order seismic wave equation. *Geophysical Journal International*, 154(1):146–153, 2003.
- [31] L. Li. Formulation and comparison of two recursive matrix algorithms for modeling layered diffraction gratings. *Journal of the Optical Society of America A*, 13:1024–1035, 1996.
- [32] L. Li. Use of fourier series in the analysis of discontinuous periodic structures. *Journal of the Optical Society of America A*, 13:1870–1876, 1996.
- [33] G. Marple, A. Barnett, A. Gillman, and S. Veerapaneni. A fast algorithm for simulating multiphase flows through periodic geometries of arbitrary shape. *SIAM Journal of Scientific Computing*, 38(5):B740–B772, 2016.
- [34] M. G. Moharam and T. G. Gaylord. Rigorous coupled-wave analysis of planar-grating diffraction. *Journal of the Optical Society of America*, 71:811–818, 1981.
- [35] C. Müller. *Foundations of the Mathematical Theory of Electromagnetic Waves*. Springer-Verlag, Berlin, New York, 1969.
- [36] M. D. Perry, R. D. Boyd, J. A. Britten, D. Decker, B. W. Shore, C. Shannon, and E. Shults. High-efficiency multilayer dielectric diffraction gratings. *Optics Letters*, 20:940–942, 1995.
- [37] V. Rokhlin. Solution of acoustic scattering problems by means of second kind integral equations. *Wave Motion*, 5:257–272, 1983.
- [38] N. Sergeant, M. Agrawal, and P. Peumans. High performance solar-selective absorbers using coated sub-wavelength gratings. *Optics Express*, 18(6):5525–5540, 2010.
- [39] Z. Sheng, P. Dewilde, and S. Chandrasekaran. Algorithms to solve hierarchically semi-separable systems. In *System theory, the Schur algorithm and multidimensional analysis*, volume 176 of *Operator Theory: Advances and Applications*, pages 255–294. Birkhäuser, Basel, 2007.
- [40] J. Xia, S. Chandrasekaran, M. Gu, and X. Li. Fast algorithms for hierarchically semiseparable matrices. *Numerical Linear Algebra with Applications*, 17(6):953–976, 2010.
- [41] J. Xia, S. Chandrasekaran, M. Gu, and X. S. Li. Superfast multifrontal method for large structured linear systems of equations. *SIAM Journal on Matrix Analysis and Applications*, 31(3):1382–1411, 2009.

APPENDIX A. THE CONSTRUCTION OF S_2

This section presents an efficient technique for constructing the tridiagonal matrix $S_2 = I + RA_0^{-1}L$.

For simplicity of presentation, let the blocks of S_2 be denoted as follows

- X_i for $1 \leq i \leq I$ denotes the diagonal blocks,
- Y_i for $2 \leq i \leq I$ denotes the lower diagonal blocks, and
- Z_i for $1 \leq i \leq I - 1$ denotes the upper diagonal blocks.

The diagonal blocks are given by

$$X_1 = \begin{bmatrix} I + R_{pm,11}A_{0,11}^{-1}L_{pm,11} & R_{pm,11}A_{0,11}^{-1}L_{12} \\ 0 & I \end{bmatrix},$$

$$X_I = \begin{bmatrix} I & 0 \\ R_{pm,II}A_{0,II}^{-1}L_{I,I-1} & I + R_{pm,II}A_{0,II}^{-1}L_{pm,II} \end{bmatrix},$$

and, for $2 \leq i \leq (I-1)$,

$$X_i = \begin{bmatrix} I & 0 & 0 \\ R_{pm,ii}A_{0,ii}^{-1}L_{i,i-1} & I + R_{pm,ii}A_{0,ii}^{-1}L_{pm,ii} & R_{pm,ii}A_{0,ii}^{-1}L_{i,i+1} \\ 0 & 0 & I \end{bmatrix}.$$

The lower diagonal blocks are given by

$$Y_2 = \begin{bmatrix} R_{21}A_{0,11}^{-1}L_{pm,11} & R_{21}A_{0,11}^{-1}L_{12} \\ 0 & 0 \end{bmatrix},$$

and, for $3 \leq i \leq I$,

$$Y_i = \begin{bmatrix} R_{i,i-1}A_{0,(i-1)(i-1)}^{-1}L_{i-1,i-2} & R_{i,i-1}A_{0,(i-1)(i-1)}^{-1}L_{pm,(i-1)(i-1)} & R_{i,i-1}A_{0,(i-1)(i-1)}^{-1}L_{i-1,i} \\ 0 & 0 & 0 \end{bmatrix}.$$

Finally the upper diagonal blocks are defined by

$$Z_i = \begin{bmatrix} 0 & 0 & 0 \\ R_{i,i+1}A_{0,(i+1)(i+1)}^{-1}L_{i+1,i} & R_{i,i+1}A_{0,(i+1)(i+1)}^{-1}L_{pm,(i+1)(i+1)} & R_{i,i+1}A_{0,(i+1)(i+1)}^{-1}L_{i+1,i+2} \end{bmatrix}$$

for $1 \leq i \leq (I-2)$, and

$$Z_{I-1} = \begin{bmatrix} 0 & 0 \\ R_{I-1,I}A_{0,II}^{-1}L_{I,I-1} & R_{I-1,I}A_{0,II}^{-1}L_{pm,II} \end{bmatrix}.$$

The matrix S_2 can be inverted via a block variant of the Thomas algorithm. Let the sum of the ranks of the low-rank approximations be defined as $N_i^{block} = k_{pm,ii} + k_{i,i-1} + k_{i,i+1}$ for $2 \leq i \leq I-1$, $N_1^{block} = k_{pm,11} + k_{1,2}$ and $N_I^{block} = k_{pm,II} + k_{I,I-1}$. The diagonal block X_i is of size $N_i^{block} \times N_i^{block}$. The upper diagonal block Z_i has size $N_i^{block} \times N_{i+1}^{block}$. The lower diagonal block Y_i has size $N_i^{block} \times N_{i-1}^{block}$.

When the i th interface is discretized to achieve a specified accuracy, N_i^{block} is a number of the number of discretization points. For the tested geometries and wave numbers, N_i^{block} is only several hundreds and can be inverted rapidly via dense linear algebra. If all of the blocks are of similar size $N_i^{block} \approx N^{block}$, then the cost inverting S_2 via the block Thomas algorithm is $\mathcal{O}([N^{block}]^3 I)$. In other words, it is linear with respect to the number of interfaces.